ISSN 1024-8560, Atmospheric and Oceanic Optics, 2024, Vol. 37, No. 4, pp. 492–501. © Pleiades Publishing, Ltd., 2024.
Russian Text © The Author(s), 2024, published in Optika Atmosfery i Okeana.

REMOTE SENSING OF ATMOSPHERE, HYDROSPHERE, AND UNDERLYING SURFACE

The Use of the Turbulent Lidar for Aviation Safety

I. A. Razenkov[a], *, B. D. Belan[a], **, A. V. Mikhal'chishin[b], *, and G. A. Ivlev[a], ******

[a] *V.E. Zuev Institute of Atmospheric Optics, Siberian Branch, Russian Academy of Sciences, Tomsk, 634055 Russia*
[b] *Siberian Scientific Research Institute of Aviation, Novosibirsk, 630051 Russia*
**e-mail: lidaroff@iao.ru*
***e-mail: bbd@iao.ru*
****e-mail: lib2005@ngs.ru*
*****e-mail: ivlev@iao.ru*

Received September 1, 2023; revised October 20, 2023; accepted October 22, 2023

Abstract—Clear air turbulence (CAT) constitutes the highest danger for aviation in the free atmosphere in the altitude range 6–12 km. Intermittence and random localization of CAT in a quiet surrounding air flow significantly restrict possibilities of its forecasting. Creation of systems for remote detection of turbulent zones becomes especially topical with allowance for climate changes and increase in the probability of CAT appearance. Results of turbulence sounding by the BSE-5 UV lidar from the Optik Tu-134 aircraft laboratory are presented. The in-flight experiment was conducted in September 2022 as part of the Arctic exploration program. The lidar recorded zones of moderate turbulence in the lower troposphere where the probability of turbulence is maximum; isolated cases of CAT were also recorded at an altitude of 9 km. The turbulent lidar can be used in practice for remote detection of turbulent zones at altitudes where most commercial flights are carried out. The prospects of ground-based application of the turbulent lidar for solving aviation safety problems during flights in the lower troposphere are also shown. The results of the BSE-5 lidar sounding in winter, when an increase in the intensity of turbulence in the 0.4–1.6-km layer was recorded during the passage of a cold front, are presented.

Keywords: turbulent lidar, backscattering enhancement, Kelvin–Helmholtz instability, clear air turbulence
DOI: 10.1134/S1024856024700660

INTRODUCTION

Clear air turbulence (CAT) means turbulent zones (spots) in a clear free atmosphere in the absence of convective motions, as well as turbulence in cirrus clouds [1]. Such turbulence appears as a result of hydrodynamic instability of an air flow stratified in speed and temperature and is characterized by intermittence and strong variability in both size and lifetime [2]. Dimensions of turbulent spots can exceed 100 km along the horizontal and 1 km in the vertical [3]. CAT often exists for a long time; therefore, several aerial vehicles (AVs) can undergo bumpiness when they successively fly through the same turbulent zone. In the upper troposphere, repeatability of CAT causing aircraft bumpiness is highest at altitudes of 6–11 km and amounts to 15% [4].

Clear air turbulence constitutes a danger for AVs because it is not recorded by aircraft systems and cannot be detected visually. Usually, CAT leads to unexpected strong bumpiness; however, cases of full destruction of the aerial vehicle were also reported. According to the ICAO Safety Report data for 2019 in 16 categories of flight accidents, the largest number of flight accidents (26%) that entailed serious injuries of air crew and passengers occurred as a result of turbulence [5].

In the ex-USSR, works on creating devices for CAT detection began in late 1980s; however, the funding was cut off after disintegration of the country. Abroad, investigations of systems for advance warning about proximity of turbulence zones continued. Since 2001, the Japan Aerospace Exploration Agency (JAXA), jointly with Mitsubishi Electric, created an aircraft lidar (the SafeAvio project) the operation principle of which is based on the Doppler effect. Later, JAXA improved the lidar, which increased the sounding range from 2 (2002) to 17 km (2017). In parallel to this, Japanese scientists decreased the weight of the system from 150 (2011) to 84 kg (2018) [6, 7]. The intensity of turbulence is estimated by a Doppler lidar by comparing the current velocity vector of the air flow with the previous value of the velocity [8]. The implementation of this approach faces a series of problems. First, the echo signal in Doppler lidars is formed only by aerosol particles which are few in number in clear air at the abovementioned altitudes [9]. Second, it is difficult to exactly determine the Doppler spectrum broadening, which also yields information about

the turbulence intensity. It was reported that the JAXA Doppler lidar had passed the tests on Boeing 777 and its certification was initiated. No information on how the JAXA Doppler system tests ended was found either in the public or in scientific literature.

Another way of CAT detection is based on recording density fluctuations of an air flow. It was implemented within the FP-7 DELICAT European project (2009–2014) on a Cessna Citation-2 aircraft [10]. This way presupposes using a high spectral resolution lidar for extracting the molecular component from the received total echo signal. The equipment created turned out to be bulky and complex, in particular, due to the presence of a powerful laser and the necessity of permanent control of the strictly horizontal position of the laser beam. The aim of the DELICAT project was to demonstrate the technology of CAT detection and did not presuppose creation of a prototype for aviation [10].

This paper presents a laser system intended for registration of turbulence intensity and CAT detection. It is alternative to the approaches outlined above. In 1972, in the Obukhov Institute of Atmospheric Physics, it was proved theoretically that if a wave propagating in a random medium is scattered in the backward direction, then the mean intensity of scattered light increases on the source axis [11]. A.S. Gurvich and colleagues [12] corroborated this experimentally in a laboratory and, later, proposed to use the phenomenon of backscattering enhancement (BSE) for remote control of optical turbulence intensity. The first working model of a turbulent lidar based on the BSE effect was created in the Zuev Institute of Atmospheric Optics in 2013. The lidar operates on molecular and aerosol scattering and allows one to remotely record the atmospheric turbulence intensity [13].

Using the BSE effect presupposes recording the scattered light intensity at the location of the radiation source. Measurements of the intensity of light scattered by a turbulent atmosphere on the axis of the probing laser beam required using a micropulse diode-pumped laser, which made it possible to combine the transmitting channel with the receiving one without overloading the detector by the laser radiation scattered by the optical elements. Note that the average output power of the micropulse laser, in combination with small dimensions, is quite acceptable and amounts to hundreds of milliwatts due to high pulse repetition frequency. In addition, the advantage of micropulse laser systems is that they are eye-safe and the resource of its continuous operation is not less than a year.

The present-day level of the technique for remote sensing of optical turbulence based on the backscattering enhancement effect permitted us to carry out flight testing with the use of the BSE-5 lidar on board the Optik Tu-134 aircraft laboratory.

The aim of this work is to introduce the reader to first results on lidar detection of turbulence in the lower troposphere and in clear air and to outline a plan for the work which seems important to us for the future.

1. MATERIALS AND METHODS

1.1. Turbulent Lidar as a Tool for Detection of CAT

The flight experiment involved the BSE-5 UV turbulent lidar [14] the simplified optical scheme of which is presented in Fig. 1. The lidar has one transmitting channel and two receiving channels: main, evenly aligned with the transmitting one, and additional, adjacent to it. The system uses one afocal telescope (the Mersenne system) consisting of a pair of parabolic mirrors *5* and *6*. The receiving channels are placed symmetrically on both sides relative to the optical axis of the telescope. Weakly diverging linearly polarized beam *2* from laser *1* passes through thin-film polarizer *3* and quarter-wave plate *4* which converts linear polarization of the laser radiation to circular polarization. Further, beam *2* is expanded by telescope *5–6* and sent into the atmosphere through the upper hole in screen *7*. Screen *7* has two similar round holes placed symmetrically relative to the telescope axis.

The radiation scattered in the atmosphere in the form of main beam *8* and additional beam *9* returns to telescope *5–6*. Beams *8* and *9* are constricted and pass through quarter-wave plate *4* which converts circular polarization of the scattered radiation back to linear polarization; now, however, the polarization plane is turned around 90° relative to laser polarization. Therefore, beams *8* and *9* are reflected from thin-film polarizer *3* and directed by mirror *10* to the receiving module which contains interference light filter *11* cutting off the background illumination; former of the lidar field of view consisting of focusing lens *12* and aperture diaphragm *13*; and photoreceivers *14* and *15* for detection of echo signals of the main and additional receiving channels *8* and *9*, respectively.

Figure 2a presents a photograph of the BSE-5 lidar with removed top cover and side plank in the laboratory; Fig. 2b, on board the Optik Tu-134. The lidar is installed opposite the emergency escape hatch on port side of the aircraft. The standard plastic window of the hatch is replaced by thick optical silica glass. The sounding path is directed perpendicularly to the fuselage. The main characteristics of the lidar are presented in Table 1.

The turbulent lidar detects the echo signal of the main receiving channel $P_1(x)$ and additional echo signal $P_2(x)$. In processing the lidar data, the echo signal $P_1(x)$ is normalized to the echo signal $P_2(x)$ to exclude the influence of the change in the scattering coefficient along the sounding direction x. When the laser beam propagates in a turbulent atmosphere, the total power of backscattered radiation does not change but

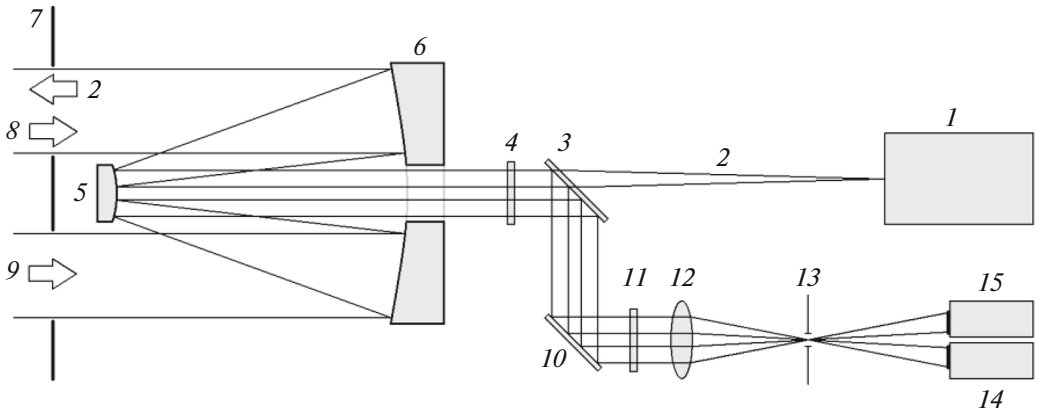

Fig. 1. Simplified optical scheme of the BSE-5 lidar. For the notation, see the text.

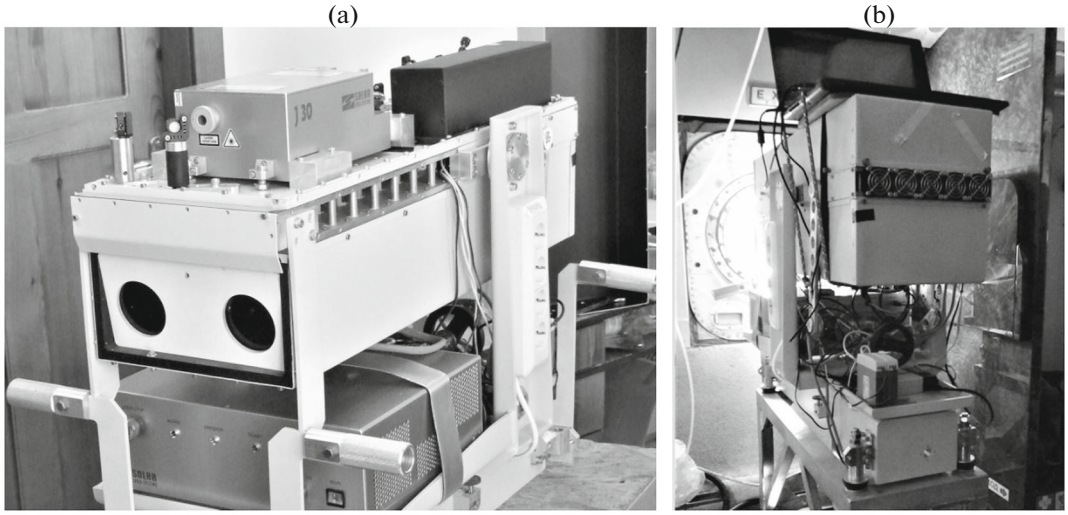

Fig. 2. BSE-5 lidar (a) indoors and (b) onboard the Optik Tu-134 aircraft laboratory.

is only redistributed in the space [15]. The mean radiation intensity increases on the laser beam axis; as a result, the echo signal P_1 increases in the main receiving channel. The profile of the structure characteristic of the refractive index $C_n^2(x)$ along the sounding path from the ratio of echo signals $P_1(x)$ and $P_2(x)$ is determined using the Vorob'ev approximation [16] with a refined constant of 3.0 instead of 0.49:

$$C_n^2(x) = \frac{q(x)\left[1 + 0.4\dfrac{r^2}{r_{\mathrm{F}}^2(x)}\right]^{7/6}}{3.0k_0^{7/6}x^{11/6}}, \qquad (1)$$

where r is the radius of the receiving aperture; $q(x) = P_1(x)/P_2(x) - 1$ is the factor of turbulence influence on the average power of scattered light at the receiver; $r_{\mathrm{F}}(x) = \sqrt{x/k_0}$ is the Fresnel scale; $k_0 = 2\pi/\lambda$ is the wavenumber; and λ is the laser radiation wavelength.

1.2. Model Calculation of Echo Signals of the Turbulent Lidar

Figure 3a presents the model distributions of the parameter $C_n^2(x)$ for a statistically homogeneous turbulence (model 1, $C_n^2(x) = \mathrm{const}$) and in the presence of a turbulent zone at a distance of 10 km from the lidar (model 2). The background value of the parameter $C_n^2 = 10^{-17}$ m$^{-2/3}$ in the model in Fig. 3 corresponds to the value of C_n^2 in the Hufnagel–Valley model at an altitude of 10 km [17]. Figure 3b presents the echo signals calculated using the transfer equation for models 1 and 2 in Fig. 3a. The turbulent zone begins at a distance of 10 km; the parameter C_n^2 grows linearly and increases by ten times at a distance of 18 km from the lidar. The echo signal of the main channel $P_1(x)$ also increases by more than an order of magnitude in the presence of a turbulent zone.

Table 1. Main characteristics of the BSE-5 lidar

Characteristic	Value	Characteristic	Value
Transmitter		*Receiver*	
Laser	Solar JX-330	Mirror afocal telescope	Mersenne (12.5×)
Wavelength, nm	355	Telescope dimensions (L × W × H), mm^3	260 × 110 × 650
Pulse duration, ns	30	Number of receiving channels	2
Repetition frequency, kHz	8	Receiver aperture, mm	70
Laser power, mW	400	Space between axes of the receiving channels, mm	150
Energy per pulse, μJ	50	Field of view of the receiving channels, μrad	400
Beam quality, $M^2 < 1.2$	TEM_{00}	Spatial resolution, m	15
Beam size ($\sim 1/e^2$), mm	70	Echo signal accumulation time, s	from 10
Beam divergence, μrad	< 30	Photoreceiver	PMT (30%)
Lidar dimensions (L × W × H), mm^3	850 × 280 × 320	Interference filter, nm	0.15

This calculation shows that in the ideal case, i.e., in the absence of noises, detection of a turbulent zone seems to be quite possible because one can expect a multiple increase in the echo signal. In a real experiment, however, the noise is always present due to various causes. The dashed line in Fig. 3a shows an arbitrarily chosen threshold value $C_n^2 = 5 \times 10^{-17}$ m$^{-2/3}$ which may be refined later. Values of C_n^2 below the chosen threshold may be ignored in the analysis of real data because the error in determining C_n^2 here is large.

2. RESULTS AND DISCUSSION

2.1. Experiment with the Lidar Onboard Tu-134

In September 2022, a complex experiment was carried out with the aim of studying the change in the air composition and characteristics of the underlying surface in the region of West Siberia and Kara Sea. It included synchronous ground-based, shipborne, and airborne measurements. When performing the main task of the experiment during the flights, the aircraft often changed the level (altitude) from 200 m to 9 km. Note that CAT sounding was not a priority task. Besides, the sounding path was directed not along the flight course but sidewise at an angle of 90°.

The turbulent lidar operated continuously in automatic mode: it was switched on beforehand on the ground and switched off after landing. The laser pulses were sent into the atmosphere with a frequency of 8 kHz, which corresponded to the maximum sounding range of 18.8 km. The echo signals coming from the atmosphere were registered in the photon-counting mode and accumulated during 10 s. then, the received signals were recorded on an individual file and the operation cycle repeated.

The KompaNav-5.2 multichannel flight data recorder system operating on board the Tu-134 formed information packages including the accelerometer data, air velocity, pressure, etc. with a frequency of 50 Hz. The lidar data were compared with acceleration (bumpiness) parameters using the vertical acceleration recorded by the KompaNav-5.2 system. Acceleration of the vertical component of the air flow and acceleration magnitude in the aircraft center of mass are connected by a relationship dependent on many parameters such as the bearing surface area of the AV (wing, fins, and fuselage), aircraft mass, air density, and others. Here, we restrict ourselves to empirical data on the relation between the AV bumpiness degree with incremental acceleration Δn in fractions of the acceleration of gravity $g = 9.81$ m/s^2 presented in Table 2 [2].

Figure 4 presents data of the flight on September 10, 2022, during 4 h by way of Salekhard–Kara Sea–Salekhard. During first 30 min, the aircraft was on the ground. On the time axis, the zero mark corresponds to 06:04 UTC. Note that beginning from the 100th minute, the fight went over the Kara Sea until leaving the altitude of 9 km at the 210th minute.

The full implementation of vertical acceleration in units of g according to KompaNav-5.2 data consisting of 720000 samples is shown in Fig. 4a. The maximum value of the vertical acceleration modulus during the flight were 3.8 m/s^2. The corresponding maximum incremental accelerations in units of g did not exceed $\Delta n = \pm 0.4$ (Fig. 4a). According to Table 2, the ride quality observed in the flight did not exceed $b^{(2)}$. It was mainly $b^{(1)}$ because $|\Delta n| < 0.2$.

The implementation of the vertical acceleration (Fig. 4a) was divided into segments equal to 1 min. For each segment, the spectrum was calculated using the fast Fourier transform. Vibrations of the aircraft body occur at relatively high frequencies, >1 Hz; for this reason, the lidar data were compared with the accelerometer by the spectral estimate at a frequency of 0.1 Hz (Fig. 4b).

From Figs. 4a and 4b one can conclude that $b^{(2)}$ took place on takeoff, landing, and flight at an altitude of 200 m; at an altitude of 9 km, $b^{(1)}$ mainly took place. Note that the accelerometer registers not only bumpiness but also aircraft body vibrations which can exceed usual values due to the aircraft age and component fatigue. When flying at an altitude of 200 m, an increase in vibrations is observed every time to values $\Delta n = \pm 0.2$, apparently due to a decrease in the AV speed and an increase in air density.

Throughout the whole experiment of September 10, 2022, the aircraft was in level flight three times at the altitude of 200 m and three times at the altitude of 9 km; the KompaNav-5.2 each time showed approximately the same values for vibrations for each altitude. This fact gives grounds to believe that under light bumpiness the accelerometer in reality detected mainly vibrations of the aircraft body, all the more so as the sensor was placed in the rear end of the Tu-134 closer to the engine unit. Therefore, the accelerometer could detect only levels beginning from $b^{(2)}$ or even $b^{(3)}$.

The result of sounding the optical turbulence intensity by the lidar in the form of the parameter C_n^2 is shown in Figs. 4c and 4d. Since the flight was in the daytime, the background illumination was the main noise source limiting the sounding range. The spatial resolution was 60 m. To reduce the influence of noise, a median filter with a spatial window of 540 m (nine points) and time window of 50 s (5 points) was applied to the recorded data. It is evident that the daytime background of the sky was a significant interference. We cannot reduce its influence by an increase in the time of signal accumulation (averaging) because this will decrease the time of arrival at the turbulent zone before the lidar will sound the alarm about the presence of CAT along the flight course.

To suppress background illumination, the following steps can be taken: (i) to increase the transmitter power; (ii) to install a light filter blocking the background with a narrower transmission band, e.g., a Fabry–Perot interferometer; and (iii) to decrease the angle of view of the receiving system. Note that each of the steps has its pluses and minuses.

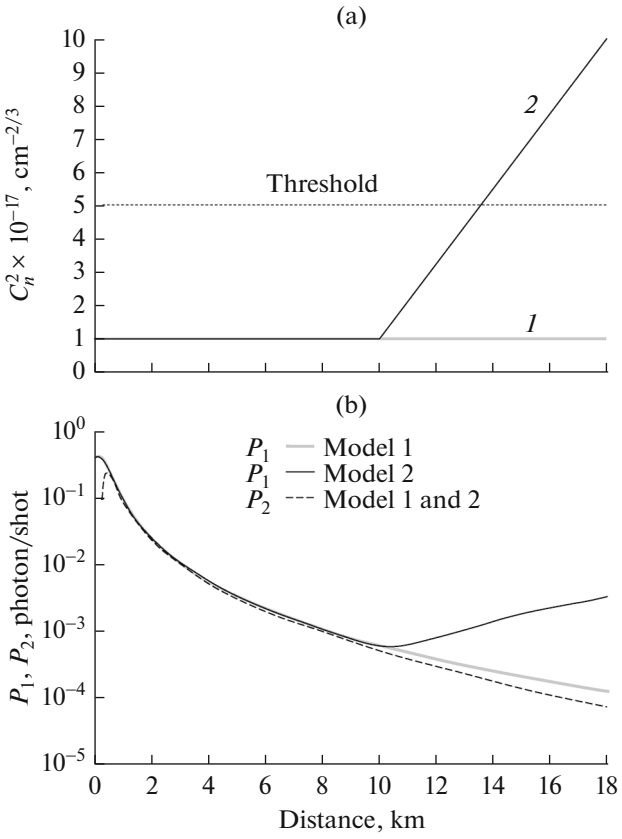

Fig. 3. (a) Models 1 and 2 of the distribution of the parameter C_n^2 along the horizontal sounding path and (b) corresponding echo signals of the main and additional receiving channels $P_1(x)$ and $P_2(x)$.

The spatiotemporal distribution of the parameter C_n^2 is presented in Fig. 4d; the shades of gray depict the changes in C_n^2 in the range $(1–30) \times 10^{-17}$ m$^{-2/3}$. Two dashed lines are also plotted here. They show the range 7.5–8.5 km for which the average values of C_n^2 were calculated. They are shown in Fig. 4c. The threshold

Table 2. Aircraft ride qualities

Ride quality	Notation	Incremental acceleration $\|\Delta n\|$
Light	$b^{(1)}$	<0.2
Moderate	$b^{(2)}$	<0.5
Severe	$b^{(3)}$	<1.0
Extreme	$b^{(4)}$	>1.0

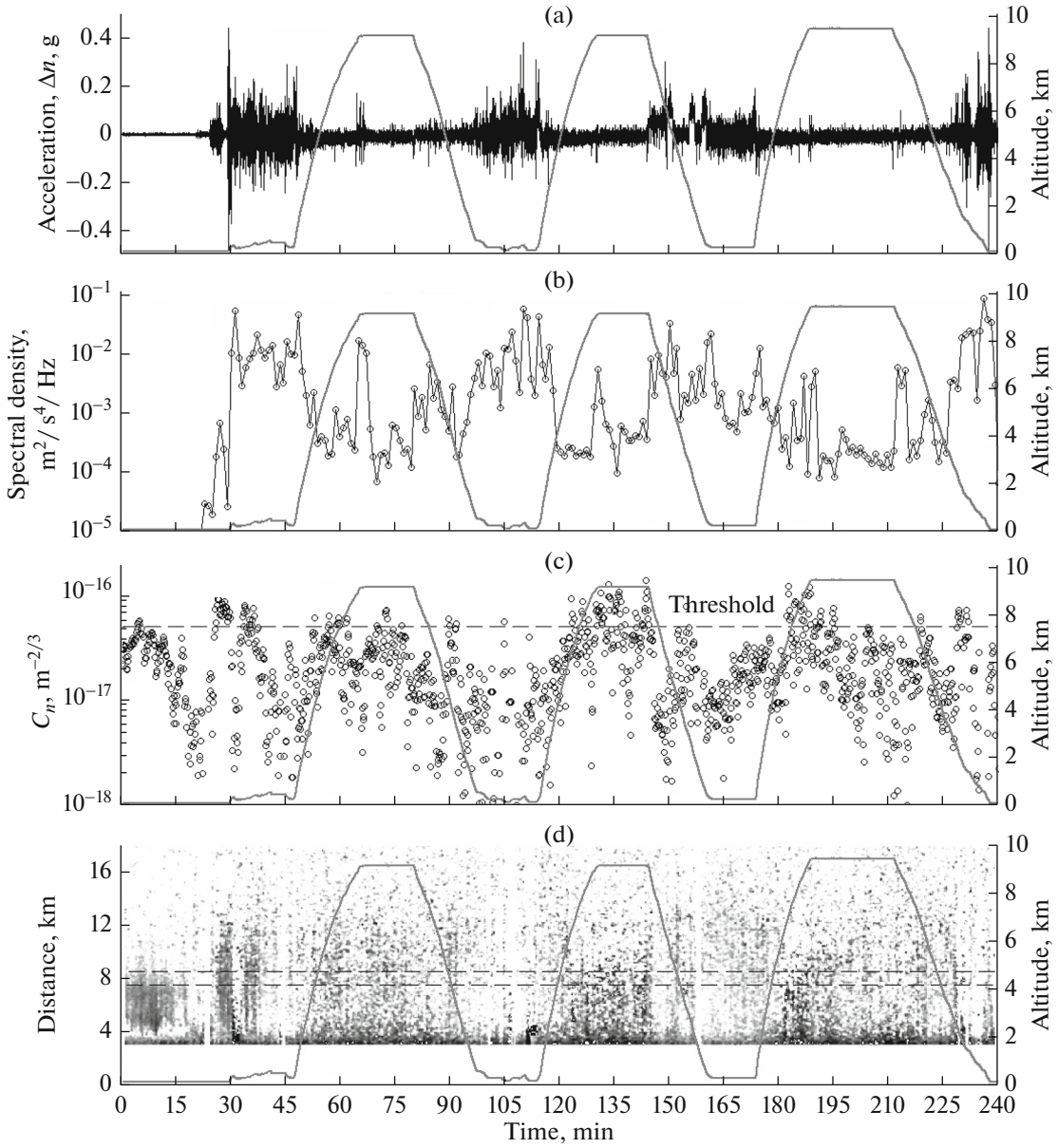

Fig. 4. (a) Time series of vertical acceleration in units of g; (b) values of the power spectrum of acceleration fluctuations at a frequency of 0.1 Hz; (c) parameter C_n^2 in the distance range of 7.5–8.5 km from the lidar; and (d) its spatiotemporal distribution with a resolution of 60 m. The solid curves are profiles of the flight altitude. The time is reckoned from 06:04 UTC Sept. 10, 2022.

$C_n^2 = 5 \times 10^{-17}$ m$^{-2/3}$ in Fig. 4c is shown by the dashed line. The maximum value $C_n^2 = 3 \times 10^{-16}$ m$^{-2/3}$ until the aircraft was on the ground.

It follows from Fig. 4c that the threshold value $C_n^2 = 5 \times 10^{-17}$ m$^{-2/3}$ (marked by the dashed line) at an altitude of 9 km was exceeded between the 130th and 150th minutes of the flight during the second lift and in the beginning of the third lift. Note that cirrus clouds were observed that time at an altitude of 9 km. The accelerometer also showed a weak increase in the vibration level (see Figs. 4a and 4b). The discrepancy between the lidar and accelerometer data can be explained by the fact that the lidar path was directed sidewise. During the lidar operation along the flight course, one could expect a better coincidence of the data but with a certain delay in time.

Figure 5 presents the data of the flight on September 11, 2022, during 4.5 h by way of Salekhard–Tomsk. During first 30 min, the aircraft was on the ground. On the time axis, the zero mark corresponds to 04:52 UTC. The full implementation of vertical acceleration in units of g consisting of 810000 samples is shown in Fig. 5a.

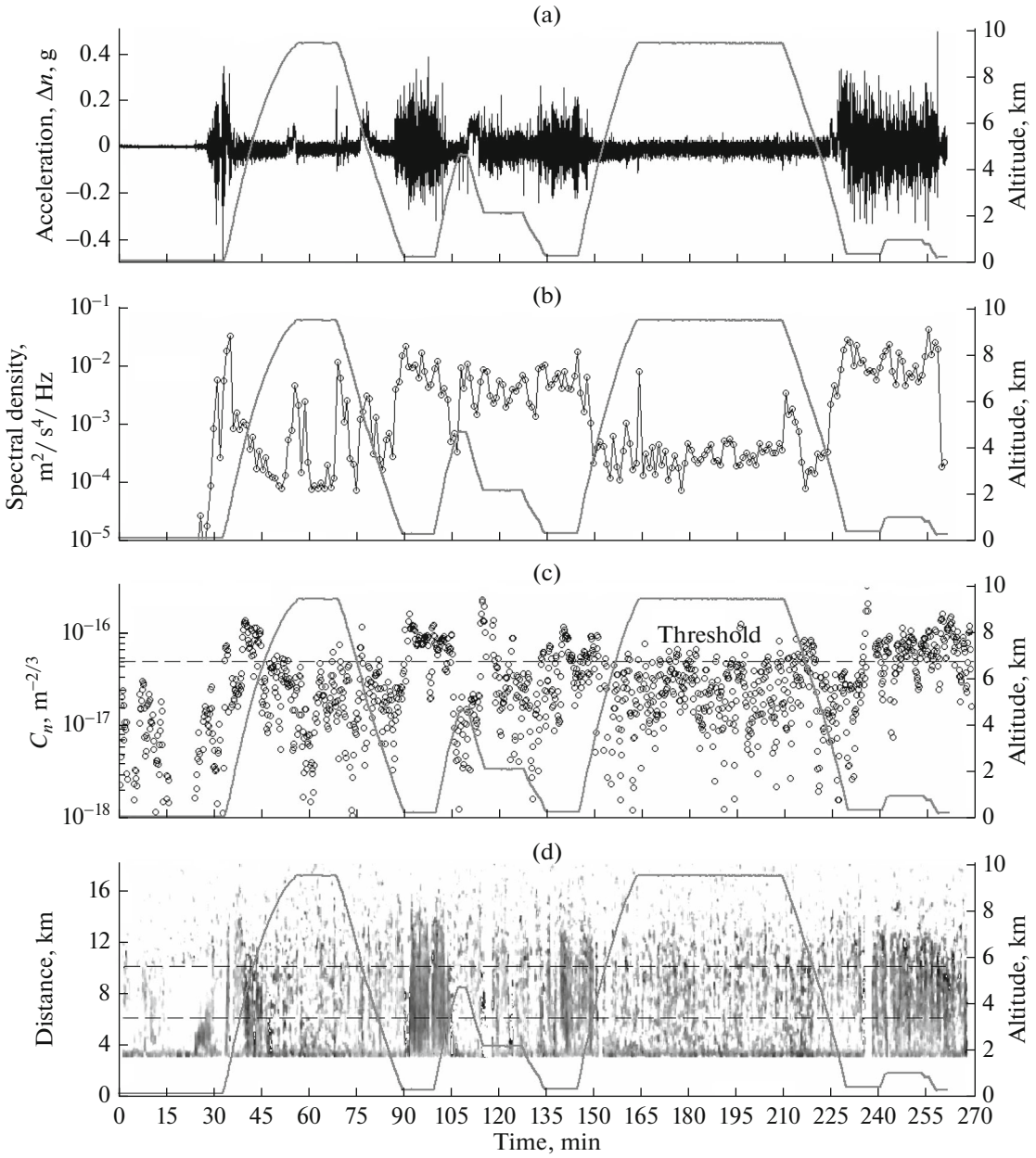

Fig. 5. Same as in Fig. 4 for the distance range 6–10 km. The time is reckoned from 04:52 UTC Sept. 11, 2022.

During the flight, the aircraft ascended to an altitude of 9 km two times; the second time, it was there for 45 min. It follows from the lidar data in Figs. 5c and 5d that only rare weak excesses of C_n^2 over the threshold value were observed, i.e., there was no pronounced CAT at large altitudes in this flight.

Nevertheless, one may distinguish in Fig. 5c four flight intervals where the parameter C_n^2 exceeded the threshold of 10^{-17} $m^{-2/3}$ during 15 min and longer. In the logbook, the time when a definite bumpiness took place in the flight was logged, namely, between the 90th and 105th minutes and after the 240th minute up to landing. Two other cases registered by the lidar may have been forgotten to be noted in the logbook. Note that this time the accelerometer in fact pointed to bumpiness synchronously with the lidar and thus demonstrated an increase in the vibration level Δn (Fig. 5a) and spectral estimate at a frequency of 0.1 Hz (Fig. 5b).

2.2. Turbulence Sounding in the Lower Troposphere

The probability to meet turbulence in the lower troposphere (0–2 km) is maximum and amounts to 25–30% on the average [1]. A ground-based experi-

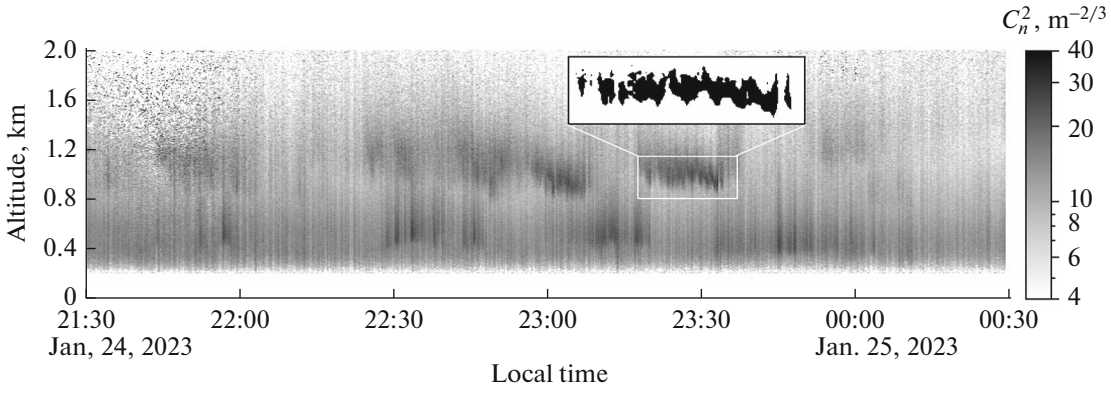

Fig. 6. Spatiotemporal distribution of the parameter C_n^2 during turbulence sounding from the ground. The BSE-5 lidar, Jan. 24–25, 2023.

ment was organized on turbulence detection with the BSE-5 lidar in the lower 2-km layer of the atmosphere. The experiment was aimed at studying the possibility to control turbulence intensity in the lower troposphere by a ground-based lidar. It is evident that the lidar operation both onboard and on the ground expands areas of its application. Measurements from the ground allow one to compare cases of turbulence appearance with the meteorological situation and thus to study justification of synoptic criteria of turbulence forecasting [1, 4].

The experiment was performed in winter. The lidar was installed indoors and operated through single-pane window glass to reduce losses. The path passed over the urban area and had a slope of 11°. The spatial resolution was 9 m; the time resolution is 10 s.

In winter, the boundary layer is usually thermally stably stratified. In the presence of a vertical gradient of wind speed and at the Richardson number less than 1/4, the Kelvin–Helmholtz instability takes place [3] and is detected by the turbulent lidar. According to our data and works of other authors [18, 19], Kelvin–Helmholtz waves appear most often in the boundary 1-km layer of the atmosphere. Turbulent zones above 1 km are detected by the ground-based lidar much less frequently.

Figure 6 presents the appearance of a turbulent zone in the form of a spatiotemporal distribution of C_n^2 detected on the night of January 24 to 25, 2023. Here, we observe two turbulized layers close to each other at altitudes of 0.4–0.8 and 0.8–1.6 km.

The inset shows a contrast image of a magnified area of the parameter C_n^2 at an altitude of 1 km recorded at 23:30. It has a pronounced wave character, which points to wave origin of the turbulent layers.

The result shown in Fig. 6 was obtained during the passage of a cold front, when the air temperature near the ground dropped from −7°C at 19:00 January 24, 2023, to −26°C at 04:00 January 25, 2023, according to data of the ICON (icosahedral nonhydrostatic) model [20]. This situation corresponds to the synoptic criterion of CAT prediction when the turbulence zone is located near the axis of the baric trough on the side of the region of low pressure [1]. Besides, a jet flow with a wind speed maximum of 21 m/s took place that time at an altitude of 1500 m [20].

Figure 7a presents 1-min-averaged echo signals P_1 (curves *1* and *3*) and P_2 (curves *2* and *4*) recorded at two time points: when the turbulent layer was present (23:22:30 January 24, 2023) and immediately after its disappearance (00:22:30 January 25, 2023). The corresponding retrieved profiles of the parameter C_n^2 are shown in Fig. 7b. The spatial resolution of the data in Fig. 7 is 45 m; the time resolution is 1 min. The profile of C_n^2 (curve *2*) in Fig. 7b represents the background value which, according to the theory, decreases with altitude by the "–4/3 law" (the dashed curve) [21]. In the turbulent layer at a distance of 6 km corresponding to an altitude of 1.2 km, a three-fold increase in C_n^2 relative to the background value was observed.

CONCLUSIONS

First experimental results of turbulence sounding by a specialized UV BSE-5 lidar installed in the Optik Tu-134 aircraft laboratory are presented. The turbulent lidar operates based on the backscattering enhancement effect, when backscattered radiation is redistributed in the space during the double passage of waves in the atmosphere and the mean radiation intensity on the laser beam axis increases.

The main results obtained by the turbulent lidar onboard the aircraft are as follows. The possibility in principle to register optical turbulence parameters up to an altitude of 9 km has been demonstrated. The sounding range in the daytime is 8–10 km (in the nighttime, measurements were not carried out). There are reasons to believe that using a 355-nm wavelength

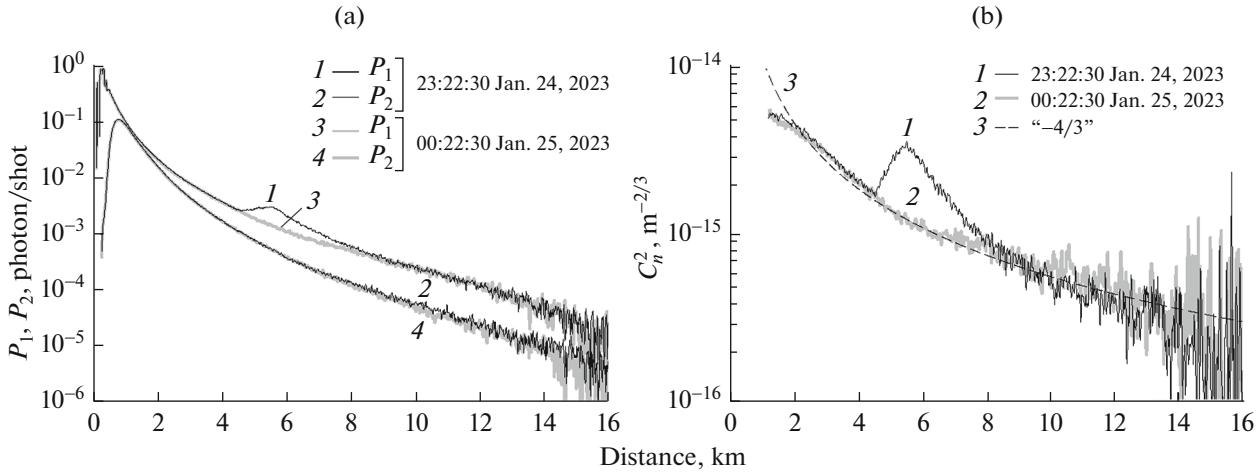

Fig. 7. (a) Echo signals P_1 (curves *1* and *3*) and P_2 (curves *2* and *4*) and (b) retrieve values of C_n^2 corresponding to them and obtained in the presence (*1*) and absence (*2*) of a turbulent zone. The theoretical profile of C_n^2 is shown by the dashed line (curve *3*). The BSE-5 lidar, Jan. 24–25, 2023.

UV laser in a turbulent lidar is optimum as compared to the visible and infrared wavelength ranges because (i) in the absence of clouds, the echo signal is larger due to molecular scattering; (ii) the sensitivity of the BSE method to a change in the turbulence intensity is higher; (iii) the radiation is eye-safe; and (iv) the radiation is invisible and thus goes unnoticed.

During the measurements, the sounding path of the turbulent lidar was directed sidewise at a right angle relative to the flight direction; therefore, the obtained results should be considered as preliminary. At present, works are being carried out on reequipment of the output port for the lidar, which will make it possible to direct the laser beam forward along the flight course. Besides, the work on creating the BSE-6 turbulent line to be mounted onboard the Tu-134 is being finalized. During the forthcoming flights, it is planned to perform long continuous measurements in the automatic mode. They will make it possible to collect experimental statistical material on lidar detection of clear air turbulence [22].

Using the turbulent lidar is not limited by its use only onboard an aerial vehicle. The ground-based lidar allows one to perform measurements in the lower troposphere. The data of sounding from the ground with the same BSE-5 lidar are presented; in winter, the slope angle of the path was 11°. The lidar could detect turbulent layers at altitudes of up to 2 km. Since the changes in the structure characteristic C_n^2 in time and space were of wave character, the Kelvin–Helmholtz instability was a possible cause of the increase in the turbulence intensity.

FUNDING

This work was supported by the Ministry of Science and Higher Education of the Russian Federation (project no. 075-15-2021-934).

CONFLICT OF INTEREST

The authors of this work declare that they have no conflicts of interest.

REFERENCES

1. *Guide to Forecasting Meteorological Conditions for Aviation* (Gidrometeoizdat, Leningrad, 1985) [in Russian].
2. N. K. Vinnichenko, N. Z. Pinus, S. M. Shmeter, and G. N. Shur, *Turbulence in the Open Atmosphere* (Gidrometeoizdat, Leningrad, 1976) [in Russian].
3. N. P. Shakina, *Hydrodynamic Instability in the Atmosphere* (Gidrometeoizdat, Leningrad, 1990) [in Russian].
4. N. P. Shakina and A. R. Ivanova, *Forecasting Meteorological Conditions for Aviation* (TRIADA, Moscow, 2016) [in Russian].
5. *Safety Report* (International Civil Aviation Organization, Montreal, Canada, 2020).
6. www.aero.jaxa.jp/eng/research/star/safeavio. Cited February 12, 2023.
7. www.oreanda.ru/en/transport/Boeing_and_JAXA_to_-Flight-test/article1173457/. Cited February 12, 2023.
8. T. Asahara and H. Inokuchi, US Patent No. US 8,434,358 B2 (May 7, 2013).
9. M. Yu. Arshinov, B. D. Belan, V. K. Kovalevskii, A. P. Plotnikov, T. K. Sklyadneva, and G. N. Tolmachev, "Long-term variability of tropospheric aerosol over Western Siberia," Atmos. Ocean. Opt. **13** (6–7), 580–583 (2000).

10. https://cordis.europa.eu/project/id/233801. Cited February 12, 2023.
11. A. G. Vinogradov, A. S. Gurvich, S. S. Kashkarov, Yu. A. Kravtsov, and V. I. Tatarskii, Inventor's Certificate no. 359. Byull. Izobret., No. 21 (1989).
12. A. S. Gurvich, "Lidar sounding of turbulence based on the backscatter enhancement effect," Izv., Atmos. Ocean. Phys. **48** (6), 585–594 (2012).
13. I. A. Razenkov, "Turbulent lidar: I—Design," Atmos. Ocean. Opt. **31** (3), 273–280 (2018).
14. I. A. Razenkov, "Engineering and technical solutions when designing a turbulent lidar," Atmos. Ocean. Opt. **35** (S1), S148–S158 (2022).
15. Yu. A. Kravtsov and A. I. Saichev, "Effects of double passage of waves in randomly inhomogeneous media," Sov. Phys. Usp. **25** (7), 494–508 (1982).
16. V. V. Vorob'ev, "On the applicability of asymptotic formulas of retrieving "optical" turbulence parameters from pulse lidar sounding data: I—Equations," Atmos. Ocean. Opt. **30** (2), 156–161 (2017).
17. V. V. Voitsekhovich, V. G. Orlov, S. Guevas, and R. Avila, "Efficiency of off-axis astronomical adaptive systems: Comparison of theoretical and experimental data," Astron. Astrophys. Suppl. Ser. **133**, 427–430 (1998).
18. I. A. Razenkov, "Sounding of Kelvin–Helmholtz waves by a turbulent lidar: I—BSE-4 lidar," Atmos. Ocean. Opt. **37** (1), 55–65 (2024).
19. M. A. Kallistratova, V. S. Lyulyukin, R. D. Kuznetsov, I. V. Petenko, D. V. Zaitseva, and D. D. Kuznetsov, "Sodar research of Kelvin–Helmholtz waves in low-level jets," in *Dynamics of Wave and Exchange Processes in the Atmosphere* (GEOS, Moscow, 2017), pp. 212–259 [in Russian].
20. https://www.ventusky.com/. Cited February 12, 2023.
21. A. S. Gurvich, A. I. Kon, V. L. Mironov, and S. S. Khmelevtsov, *Laser Radiation in a Turbulent Atmosphere* (Nauka, Moscow, 1976) [in Russian].
22. I. A. Razenkov, B. D. Belan, K. A. Rynkov, and G. A. Ivlev, RF Patent No. 2023106962, Byull. Izobret., No. 18 (2023).

Translated by A. Nikol'skii